



ELSEVIER

1 August 1996

OPTICS  
COMMUNICATIONS

Optics Communications 129 (1996) 6–12

## A fictitious photons method for tomographic imaging

Giacomo M. D'Ariano<sup>a,1</sup>, Chiara Macchiavello<sup>b,1</sup>, Matteo G.A. Paris<sup>c,1</sup>

<sup>a</sup> Department of Electrical Engineering and Computer Science, Department of Physics and Astronomy,  
Northwestern University, Evanston, IL 60208, USA

<sup>b</sup> Clarendon Laboratory, University of Oxford, Parks Road, Oxford OX1 3PU, UK

<sup>c</sup> Arbeitsgruppe 'Nichtklassische Strahlung' der Max-Planck-Gesellschaft an der Humboldt-Universität zu Berlin,  
Rudower Chaussee 5, 12489 Berlin, Germany

Received 4 September 1995; revised version received 12 February 1996; accepted 13 March 1996

### Abstract

We present a new tomographic method that is suited to imaging from very weak signals with a high resolution apparatus. The method arises from a procedure for measuring the density matrix of the radiation field, and relies on a correspondence between images and trace-class matrices. Accurate image reconstructions are achieved with relatively small numbers of data.

### 1. Introduction

The essential problem of tomographic imaging is to recover a mass distribution  $\mu(x, y)$  in a 2-d slab from a finite collection of one-dimensional projections. The situation is schematically sketched in Fig. 1a where  $\mu(x, y)$  describes two circular holes in a uniform background. The tomographic machine, say an X-ray equipment, collects many stripe photos of the sample from various directions  $\phi$ , and then numerically performs a mathematical transformation – the so-called *inverse Radon transform* [1] – in order to reconstruct  $\mu(x, y)$  from its radial profiles at different  $\phi$ . The problem which is of interest for us is when the radial profiles are not well resolved digitalized functions, but actually represent the density distribution of random points – as if in our X-ray machine the beam is so weak that radial photos are just

the collection of many small spots, each from a single X-ray photon (this situation is sketched in Fig. 1b). It is obvious that this case can be reduced to the previous one by counting all points falling in a predetermined 1-d mesh, and giving radial profiles in form of histograms (this is what actually happens in a real machine, using arrays of photodetectors). However, we want to use the whole available information from each “event” – i.e. the exact 1-d location of each spot – in a way which is independent of any predetermined mesh. In practice, this situation occurs when the signal is so weak and the machine resolution is so high (i.e. the mesh-step is so tiny) that only zero or one photon at most can be collected in each channel. As we will see in this paper, this low-signal/high-resolution case naturally brings the imaging problem into the quantum domain. Here, we have at disposal a technique [3] for measuring the density matrix of the field in terms of homodyne outcomes (the equivalent of our radial spots) for different phases of the local oscillator (the equivalent of our  $\phi$  angle). This technique – ac-

<sup>1</sup> Permanent address: Dipartimento di Fisica “Alessandro Volta”,  
via A. Bassi 6, I-27100 Pavia, Italy.

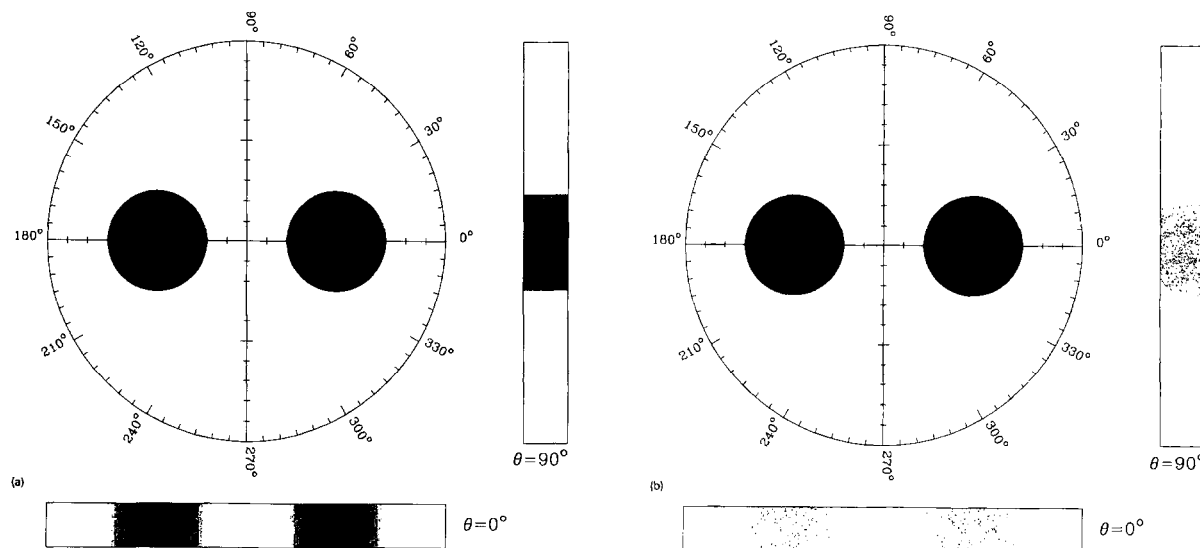


Fig. 1. (a) Tomography of a simple object: analytical transmission profiles are reported for  $\phi = 0, \pi/2$ . (b) The same case of (a), but here for very weak signals: in this case the transmission profiles are given in terms of random points on a photographic plate (here obtained from a Monte Carlo simulation).

tually called *quantum homodyne tomography* – needs no a priori mesh or cutoff [3]: the image to be recovered is just the Wigner function of the field [4], which is in one-to-one correspondence with the density matrix. Extending this correspondence to the case of customary imaging, we obtain a description of images in terms of density matrices. These are still trace-class matrices (corresponding to “normalizable” images), but are no longer positive definite, because an “image” generally is not a genuine Wigner function and violates the Heisenberg relations on the complex plane (the phase space of a single mode of radiation). Hence, such density matrices are unphysical: they are just a mathematical tool for imaging. This is the reason why we name this method *Fictitious Photons Tomography*. As we will see in the following, the image resolution improves increasing the rank of the density matrix, and in this way the present method also provides a new algorithm for image compression, which is particularly suited to angular image scanning.

After briefly recalling the customary tomographic imaging technique in Section 2, in Section 3 we briefly present the method of quantum tomography and the correspondence between density matrices and images. Section 4 analyzes the new imaging algorithm on the basis of numerical checks and Monte Carlo experi-

ments. Section 5 closes the paper with some concluding remarks.

## 2. Classical imaging

In this section we shortly review the customary imaging technique based on the filtered inverse Radon transform. In order to allow an easy comparison with the quantum case we adopt the complex notation, with  $\alpha = x + iy$  representing a point in the image plane. In this way  $\alpha$  and  $\bar{\alpha}$  are considered as independent variables, and the 2-d image – here denoted by the same symbol  $W(\alpha, \bar{\alpha})$  used for the Wigner function – is just a generic real function of the point in the plane<sup>2</sup>. In the most general situation  $W(\alpha, \bar{\alpha})$  is defined on the whole complex plane, where it is normalized to some finite constant, and it is bounded from both below and above, with a range representing the darkness nuance. For X-ray tomography  $W(\alpha, \bar{\alpha})$  roughly represents the absorption coefficient as a function of the point  $\alpha$ . (We consider a linear absorption regime, i.e. the image extension is negligible with respect to

<sup>2</sup> Usually in the complex notation  $z = f(\alpha)$  denotes a holomorphic function, whereas  $z = f(\alpha, \bar{\alpha})$  represents a generic function – i.e. both holomorphic and antiholomorphic – of  $\alpha$ .

the radiation absorption length in the medium. At the same time we neglect any diffraction effect.)

A tomography of a two-dimensional image  $W(\alpha, \bar{\alpha})$  is a collection of one-dimensional projections  $p(x, \phi)$  at different values of the observation angle  $\phi$ . The mathematical definition is given by the Radon transform of  $W(\alpha, \bar{\alpha})$ , namely

$$p(x, \phi) = \int_{-\infty}^{+\infty} \frac{dy}{\pi} W((x + iy)e^{i\phi}, (x - iy)e^{-i\phi}). \quad (1)$$

In Eq. (1)  $x$  is the current coordinate along the direction orthogonal to the projection and  $y$  is the coordinate along the projection direction. The situation is illustrated in Fig. 1 where  $W(\alpha, \bar{\alpha})$  is plotted along with its  $p(x, \phi)$  profiles for  $\phi = 0, \pi/2$  for a couple of identical circular holes that are symmetrically disposed with respect to the origin.

The reconstruction of the image  $W(\alpha, \bar{\alpha})$  from its projections  $p(x, \phi)$  – also called “back projection” – is given by the inverse Radon transform

$$W(\alpha, \bar{\alpha}) = \frac{1}{4} \int_{-\infty}^{+\infty} dk |k| \int_0^\pi \frac{d\phi}{\pi} \times \int_{-\infty}^{+\infty} dx p(x, \phi) \exp[ik(x - \alpha_\phi)], \quad (2)$$

where  $\alpha_\phi = \text{Re}(\alpha e^{-i\phi})$ . Upon exchanging integrals over  $k$  and  $\phi$ , the image  $W(\alpha, \bar{\alpha})$  can be written as a double integral

$$W(\alpha, \bar{\alpha}) = \int_0^\pi \frac{d\phi}{\pi} \int_{-\infty}^{+\infty} dx p(x, \phi) K(x - \alpha_\phi). \quad (3)$$

The kernel  $K(z)$  in Eq. (3) is given by

$$K(z) = -\frac{1}{2} P \frac{1}{z^2} \equiv -\lim_{\epsilon \rightarrow 0^+} \frac{1}{2} \text{Re} \frac{1}{(z + i\epsilon)^2}, \quad (4)$$

where  $P$  denotes the Cauchy principal value. Integrating Eq. (3) by parts, one obtains the familiar filtering procedure

$$W(\alpha, \bar{\alpha}) = \int_0^\pi \frac{d\phi}{2\pi} P \int_{-\infty}^{+\infty} dx \frac{\partial p(x, \phi) / \partial x}{x - \alpha_\phi}, \quad (5)$$

which is commonly used in conventional tomographic imaging (see, for example, Ref. [2]).

Let us now critically consider the above procedure in the case of very weak signals, namely when  $p(x, \phi)$  just represents the probability distribution of random X-ray spots on a fine-mesh multichannel: this situation is sketched in Fig. 1b. From Eq. (5) one can recover  $W(\alpha, \bar{\alpha})$  only when the analytical form of  $p(x, \phi)$  is known. But the experimental outcomes of each projection actually are random data distributed according to  $p(x, \phi)$ , whereas in order to recover  $W(\alpha, \bar{\alpha})$  from Eq. (5) one needs to evaluate first order derivatives of  $p(x, \phi)$ . The need of an analytical form for projections  $p(x, \phi)$  requires a filtering procedure on data, and this can be accomplished either by putting a high- $k$  cutoff on the Fourier transform (2), or by “splining” data in order to use Eq. (5). Eq. (3) formally gives  $W(\alpha, \bar{\alpha})$  in form of average on data, but from Eq. (4) it is apparent that the kernel  $K(z)$  is unbounded, and thus it is not suited to statistical sampling, unless boundness is artificially introduced by fixing a finite value of  $\epsilon$ .

All the above procedures lead to approximate image reconstructions, and the choice of any kind of smoothing parameter unavoidably affects in a systematic way the statistics of errors of imaging. To the knowledge of the authors there is no systematic analysis of these effects in the current literature. Moreover, such procedures are not suited to the case of sparse data, corresponding to very weak signals. In the next section we will briefly recall a quantum tomographic method that has been originally introduced in order to measure the density matrix of the radiation field without approximations. Then, in Section 4 we will show how such method can be used for conventional imaging in presence of weak signals, providing both ideally controlled resolution and reliable error statistics.

### 3. Quantum tomography

In recent papers [3,5,6] a new method to recover the density matrix  $\hat{\rho}$  of a single mode of radiation field has been developed. The method relies on measurements of the field quadratures

$$\hat{x}_\phi = \frac{1}{2}(a^\dagger e^{i\phi} + a e^{-i\phi}) \quad (6)$$

at different phases  $\phi$ , and therefore it is referred to as a *Quantum Tomography*. The novelty of this method lies on the exact computability of the density matrix, which is obtained only from averages on experimental data without any cut-off. In the quantum domain this is of great relevance, because any smoothing procedure in the phase space  $(\alpha, \bar{\alpha})$  produces systematic errors that make the state “more classical”, and prevents from detecting quantum features, such as oscillations of the photon number probability. In the following section we will come back to the problem of conventional imaging, and we will apply this method as a new technique for image reconstruction.

The starting point of quantum tomography is the operator identity

$$\hat{\rho} = \int \frac{d^2\alpha}{\pi} \text{Tr}(\hat{\rho} e^{-\bar{\alpha}a} e^{\alpha a^\dagger}) e^{-\alpha a^\dagger} e^{\bar{\alpha}a}, \quad (7)$$

which in polar coordinates  $\alpha = (i/2)re^{i\phi}$  becomes

$$\hat{\rho} = \int_{-\infty}^{+\infty} \frac{dr|r|}{4} \int_0^\pi \frac{d\phi}{\pi} \text{Tr}(\hat{\rho} e^{ir\hat{x}_\phi}) e^{-ir\hat{x}_\phi}. \quad (8)$$

Notice that the identity (7) is just the operator form of the Fourier-transform relation between Wigner function and characteristic functions for a general density matrix.

Using the resolution of the identity in terms of the eigenvectors of  $\hat{x}_\phi$  and exchanging the order of the integrals, one obtains

$$\hat{\rho} = \int_0^\pi \frac{d\phi}{\pi} \int_{-\infty}^{+\infty} dx p(x, \phi) K(x - \hat{x}_\phi), \quad (9)$$

where  $p(x, \phi)$  is the probability distribution of the field quadrature  $\hat{x}_\phi$  at the phase  $\phi$ , and the kernel  $K(z)$  has the same form given in Eq. (4). As shown in Ref. [6], although the kernel  $K(x)$  is an unbounded function (not even a tempered distribution), for some vectors  $|\psi\rangle$  and  $|\varphi\rangle$  in the Hilbert space the matrix element  $\langle\psi|K(x - \hat{x}_\phi)|\varphi\rangle$  is bounded as a function of  $x$ . This occurs in the case of the number representation, where the matrix elements  $\varrho_{n,n+d} \equiv \langle n|\hat{\rho}|n+d\rangle$  are given by

$$\begin{aligned} \langle n|\hat{\rho}|n+d\rangle &= \int_0^\pi \frac{d\phi}{\pi} \int_{-\infty}^{+\infty} dx p(x, \phi) \\ &\times \langle n|K(x - \hat{x}_\phi)|n+d\rangle, \end{aligned} \quad (10)$$

with

$$\begin{aligned} \langle n|K(x - \hat{x}_\phi)|n+d\rangle &= 2e^{-id\phi} \sqrt{\frac{n!}{(n+d)!}} e^{-x^2} \sum_{\nu=0}^n \frac{(-1)^\nu}{\nu!} \binom{n+d}{n-\nu} \\ &\times (2\nu + d + 1)! \text{Re}\{(-i)^d D_{-(2\nu+d+2)}(-2ix)\}, \end{aligned} \quad (11)$$

$D_\sigma(z)$  denoting the parabolic cylinder function of index  $\sigma$ . Then, according to Eq. (10), the reconstructed density matrix  $\varrho_{n,n+d}$  is obtained by averaging the kernel  $\langle n|K(x - \hat{x}_\phi)|n+d\rangle$  over the experimental data  $\{(x, \phi)\}$ . Typically, the average on the phase  $\phi$  is evaluated by means of a Cavalieri–Torricelli integration formula with  $F$  equally spaced phases  $\phi_f = f\pi/F$  ( $f = 0, \dots, F-1$ ).

From the density matrix  $\varrho_{n,m}$  one can obtain the Wigner function on the complex plane,

$$W(\alpha, \bar{\alpha}) = \int_{\mathbb{C}} \frac{d^2\lambda}{\pi} \text{Tr}\{\hat{\rho} e^{\lambda a^\dagger - \bar{\lambda}a}\} e^{\alpha\bar{\lambda} - \bar{\alpha}\lambda}, \quad (12)$$

where  $\alpha$  is the complex amplitude of the field. In the number representation the trace in Eq.(12) is evaluated in the form of a discrete Fourier transform

$$W(\alpha, \bar{\alpha}) = \text{Re} \sum_{d=0}^{\infty} e^{id\phi} \sum_{n=0}^{\infty} A(n, d; |\alpha|) \varrho_{n,n+d}, \quad (13)$$

$$\begin{aligned} A(n, d; |\alpha|) &= (-1)^n 2(2 - \delta_{d0}) |2\alpha|^d \\ &\times \sqrt{\frac{n!}{(n+d)!}} e^{-2|\alpha|^2} L_n^d(|2\alpha|^2), \end{aligned} \quad (14)$$

where  $L_n^d(x)$  denote Laguerre polynomials. In practice, the Hilbert space has to be truncated at some finite dimension  $d_{\mathcal{H}}$ , and this sets the resolution for the reconstruction of  $W(\alpha, \bar{\alpha})$ . However, as we will see in the following, this resolution can be chosen at will, independently of the number of experimental data.

#### 4. Quantum imaging

In this section we show how the method presented in Section 3 can be used for ordinary imaging from weak signals. In general an image does not correspond to a Wigner function of a physical state, due to the fact that the Heisenberg relations unavoidably produce only smooth Wigner functions, whereas a conventional image can have very sharp edges. For example, in the case of a uniform circle of radius  $R$  the product of uncertainties corresponding to orthogonal directions is given by

$$\langle \Delta x_\phi^2 \rangle \langle \Delta x_{\phi+\pi/2}^2 \rangle = R^4/9, \quad (15)$$

and the Heisenberg lower bound for the uncertainty product is thus violated for sufficiently small radius ( $R < \sqrt{3}/2$ ). However, if one allows the density matrix  $\varrho_{n,m}$  to be no longer positive definite (but still trace class), a correspondence between density matrices and images is obtained, which holds in general. In this way every image is stored into a trace-class matrix  $\varrho_{n,m}$  via quantum tomography, and a convenient truncation of the matrix dimension  $d_{\mathcal{H}}$  can be chosen. We emphasize again that the density matrix does not correspond to any physical state of radiation, and this is the reason why we name this method Fictitious Photons Tomography.

The connection between images and matrices is the main point of our approach: the information needed to reconstruct the image is stored in a  $d_{\mathcal{H}} \times d_{\mathcal{H}}$  matrix. For a suitably chosen dimension  $d_{\mathcal{H}}$  the present method can also provide a procedure for image compression. Notice that the correspondence between images and trace-class matrices retains some symmetries of the image, which manifest as algebraic properties of the matrix  $\varrho_{n,m}$ . For example an isotropic image (like a uniform circle centered at the origin) is stored in a diagonal matrix. Other symmetries are given in Table 1.

The truncated Hilbert space dimension  $d_{\mathcal{H}}$  sets the imaging resolution. The kind of resolution can be understood by studying the behavior of the kernels  $\langle n|K(x - \hat{x}_\phi)|n+d\rangle$  in Eq. (11) which are averaged over the experimental data in order to obtain the matrix elements  $\varrho_{n,n+d}$ . Outside a region that is almost independent of  $n$  and  $d$ , all functions  $\langle n|K(x - \hat{x}_\phi)|n+d\rangle$  decrease exponentially, whereas inside this region they

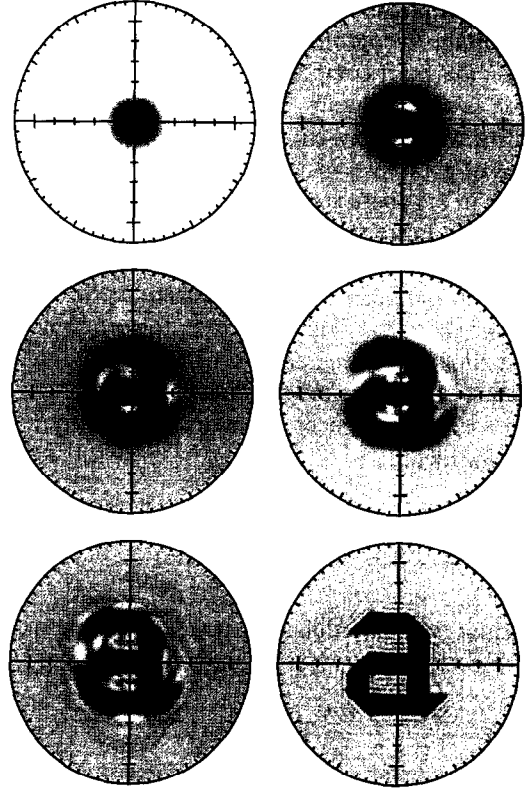


Fig. 2. Tomographic reconstruction of the font “a” for increasing dimension of the truncated matrix,  $d_{\mathcal{H}} = 2, 4, 8, 16, 32, 48$ . The plot is obtained by integrating numerically Eq. (10), from analytically assigned transmission profiles  $p(x, \phi)$ , and then using Eq. (13).

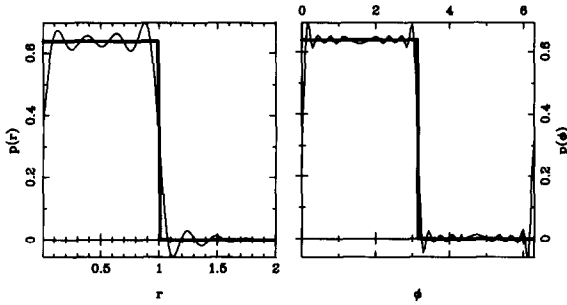
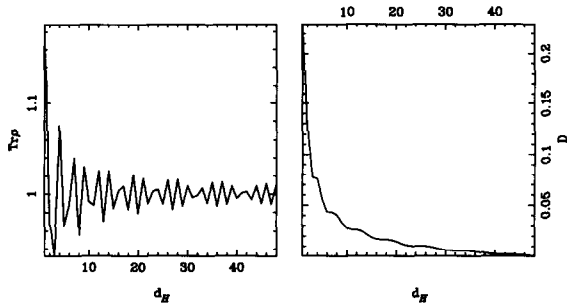
oscillate with a number of oscillations linearly increasing with  $2n + d$ . This behavior produces the effects illustrated in Fig. 2, where we report the tomographic reconstruction of the font “a” for increasing dimension  $d_{\mathcal{H}}$ . The plot is obtained by numerically integrating Eq. (10) from analytically given transmission profiles  $p(x, \phi)$ , and after using Eq. (13). As we see from Fig. 2 both the radial and the angular resolutions improve versus  $d_{\mathcal{H}}$ , making the details of the image sharper and sharper. Due to limitations in numerical precision the maximum rank that we can currently reach is  $d_{\mathcal{H}} = 48$ .

For this maximum resolution in Fig. 3 we report the radial and the angular profiles corresponding to the imaging of a semicircle with unit radius centered at the origin: one can see that the precision of the reconstruction stays within 5% from the exact profiles.

Table 1

Geometrical symmetries of an image, analytical properties of projections and algebraic properties of the corresponding matrix

Symmetry	$p(x, \phi)$	$\varrho$
Isotropy	$p(x, \phi) \equiv p(x)$	$\varrho_{n,m} = \rho_{n,n} \delta_{n,m}$
X-axis mirror	$p(x, \pi - \phi) = p(-x, \phi)$	$\varrho_{n,m} \in \mathbb{R}$
Y-axis mirror	$p(x, \pi - \phi) = p(x, \phi)$	$i\varrho_{n,m} \in \mathbb{R}$
Inversion through the origin	$p(x, \phi) = p(-x, \phi)$	$\varrho_{n,n+2d+1} = 0$

Fig. 3. Radial and angular profiles ( $p(r)$  and  $p(\phi)$  respectively) of the reconstructed image of a uniform semicircle of unit radius centered at the origin. Matrix elements are obtained as in Fig. 2.Fig. 4. Convergence of both trace and Hilbert distance  $D$  in Eq. (16) versus the dimensional truncation  $d_{\mathcal{H}}$  of the Hilbert space. Here the image is a uniform circle of unit radius centered at the origin. The reconstructed matrix elements are obtained as in Fig. 2, whereas the exact matrix elements are provided by Eq. (17).

A quantitative measure of the precision of the tomographic reconstruction can be given in terms of the distance  $D$  between the true and the reconstructed image, which, in turn, coincides with the Hilbert distance  $D$  between the corresponding density matrices. One has

$$D = \int d^2\alpha |\Delta W(\alpha, \bar{\alpha})|^2 = \text{Tr}(\Delta \hat{\rho})^2$$

$$= \sum_{n=0}^{\infty} \Delta \varrho_{n,n}^2 + 2 \sum_{n=0}^{\infty} \sum_{\lambda=1}^{\infty} |\Delta \varrho_{n,n+\lambda}^2|^2, \quad (16)$$

where  $\Delta[\dots] = [\dots]_{\text{true}} - [\dots]_{\text{reconstructed}}$ . The convergence of  $D$  versus  $d_{\mathcal{H}}$  is given in Fig. 4 for a solid circle of unit radius centered at the origin. In this case the exact density matrix can be obtained from Eqs. (10) and (11), and according to Table 1 it has only diagonal elements. These are given by

$$\varrho_{n,n} = 2 \sum_{\nu=0}^n (-2)^{\nu} \binom{n}{\nu} \Phi(1-\nu, 2, 2R^2), \quad (17)$$

with  $\Phi(\alpha, \beta, z)$  denoting the confluent hypergeometric function of argument  $z$  and parameters  $\alpha$  and  $\beta$ .

Insofar we have analyzed our method only on the basis of analytically given profiles  $p(x, \phi)$ . As already said, however, the method is particularly advantageous in the weak-signal/high-resolution situation, where the imaging can be achieved directly from averages on data according to Eqs. (10), (11) and (13). In this case our procedure allows to exploit the whole available experimental resolution, whereas the image resolution is set at will. In Fig. 5 we report a Monte Carlo simulation of an experimental tomographic reconstruction of the font “a” for increasing number of data. All plots are obtained at the maximum available dimension  $d_{\mathcal{H}} = 48$ , and using  $F = 100$  scanning phases. The situation occurring for small numbers of data is given in the first plot, where the highly resolved image still exhibits the natural statistical fluctuations due to the limited number of data. For larger samples the image starts to appear more and more sharply from the random background, and it is clearly recognizable for a total number of data equal to  $10^6$ . Moreover, the present method is very efficient also from the compu-

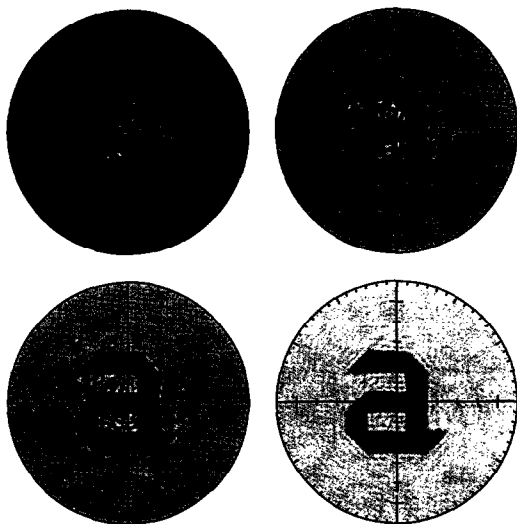


Fig. 5. Monte Carlo simulation of an experimental tomographic reconstruction of the font "a". The truncation dimension is fixed at  $d_H = 48$ , and the number of scanning phases is  $F = 100$ . The plots correspond to  $10^3, 10^4, 10^5, 10^6$  data for each phase respectively.

*tational complexity point of view, as the time needed for image reconstruction is quadratic in the number of elements of the density matrix and linear in the number of experimental data.*

## 5. Conclusions

In this paper we have presented a novel method for tomographic imaging. The method generalizes a recently proposed procedure to measure the density matrix of the radiation field, and relies on a correspondence between images and trace-class matrices.

Image reconstruction is obtained by means of averages on experimental data, without any kind of smoothing or filtering procedure. In this way the method becomes particularly suited to the low-signals/high-resolution regime, when only few experimental data are at disposal and one wants to exploit the full available machine resolution. Monte Carlo tests indicate accurate image reconstructions with relatively small numbers of data.

## References

- [1] F. Natterer, *The mathematics of computerized tomography* (Wiley, 1986).
- [2] P. Mansfield and P.G. Morris, *NMR Imaging in Biomedicine* (Academic Press, 1982).
- [3] G.M. D'Ariano, C. Macchiavello and M.G.A. Paris, *Phys. Rev. A* 50 (1994) 4298;  
The experimental feasibility of optical homodyne tomography to detect density matrix of radiation was given by D.T. Smithey, M. Beck, M.G. Raymer and A. Faridani, *Phys. Rev. Lett.* 70 (1993) 1244 (however, this method was based on the Radon transform technique).
- [4] For a review on Wigner functions see M. Hillery, R.F. O'Connell, M.O. Scully and E.P. Wigner, *Phys. Rep.* 106 (1984) 121.
- [5] G.M. D'Ariano, C. Macchiavello and M.G.A. Paris, *Nuovo Cimento B* 110 (1995) 237.
- [6] G.M. D'Ariano, U. Leonhardt and H. Paul, *Phys. Rev. A* 52 (1995) (in press).